nature geoscience

ARTICLES

https://doi.org/10.1038/s41561-022-00942-1

Check for updates

OPEN

Global cycling and climate effects of aeolian dust controlled by biological soil crusts

E. Rodriguez-Caballero[1,2]✉, T. Stanelle[3,13], S. Egerer[4,14], Y. Cheng[5], H. Su[2], Y. Canton[1,6], J. Belnap[7], M. O. Andreae[8,9,10], I. Tegen[11], C. H. Reick[4], U. Pöschl[2] and B. Weber[2,12]✉

Biological soil crusts (biocrusts) cover ~12% of the global land surface. They are formed by an intimate association between soil particles, photoautotrophic and heterotrophic organisms, and they effectively stabilize the soil surface of drylands. Quantitative information on the impact of biocrusts on the global cycling and climate effects of aeolian dust, however, is not available. Here, we combine the currently limited experimental data with a global climate model to investigate the effects of biocrusts on regional and global dust cycling under current and future conditions. We estimate that biocrusts reduce the global atmospheric dust emissions by ~60%, preventing the release of ~0.7 Pg dust per year. Until 2070, biocrust coverage is expected to be severely reduced by climate change and land-use intensification. The biocrust loss will cause an increased dust burden, leading to a reduction of the global radiation budget of around 0.12 to 0.22 W m^{-2}, corresponding to about 50% of the total direct forcing of anthropogenic aerosols. This biocrust control on dust cycling and its climate impacts have important implications for human health, biogeochemical cycling and the functioning of the ecosystems, and thus should be considered in the modelling, mitigation and management of global change.

About 25% of the dryland soil surfaces, corresponding to 12% of the global land surface, are currently covered by biological soil crusts (biocrusts)[1]. Although these communities represent a small fraction of the soil profile, they contribute to the biogeochemical cycling of nutrients, serving as nitrogen and carbon sources and improving the soil water balance and plant growth[1–6]. They also emit nitric oxide (NO) and nitrous acid (HONO)[7,8], which influence the ozone production and OH reactivity of the atmosphere[9,10]. Biocrust organisms grow on top or within the uppermost millimetres of the soil, shielding the soil surface and entangling soil particles with their rhizines and hyphae. Many biocrust-forming organisms secrete extracellular polymeric substances, consisting of amino acids, polysaccharides and other carbohydrates, which agglutinate the soil particles[11]. All these stabilizing effects cause biocrusts to form a strongly armoured cohesive layer, which increases soil resistance against erosion, thus preventing soil particle and nutrient mobilization[12].

Atmospheric dust represents a key component of aerosols, which are relevant in climate processes, with the exact effects still to be determined[13]. Most dust is generated by aeolian erosion in drylands at rates that depend on surface conditions and meteorology and may shift in a changing climate[14]. Upon emission, dust may be transported over long distances before deposition[15]. During transport, dust particles influence the optical properties of the atmosphere as they scatter incoming solar radiation and absorb long-wave emissions[16]. They also serve as ice and cloud condensation nuclei[17] and are chemically altered by processes within the atmosphere[18,19]. Dust contains nutrients and organic matter from source areas, which, upon deposition, can potentially increase productivity of nutrient-depleted ocean and land ecosystems, modifying regional and global biogeochemical cycles[20–22]. When deposited on snow and glacier surfaces, dust enhances the absorption of solar radiation and melting rates of snow, with negative impacts on freshwater supplies and the phenology of alpine vegetation[23]. Dust particles may also negatively influence human health by carrying pathogens (for example, viruses, bacteria and fungi), triggering respiratory and cardiovascular diseases and causing highway accidents[20]. In controlled wind simulation experiments, biocrusts have been shown to effectively decrease dust emissions, but these were focused on small-scale process studies[24,25]. The impact of biocrusts on the global dust cycle has yet to be determined.

In this study, we used the currently limited existing experimental data of biocrust effects on threshold friction velocities (TFVs), the minimum wind velocity at which soil particles start being dislodged from the matrix (Supplementary Table 1). On the basis of these data, we used exponential relationships (as previously described by ref. [25]) to describe the mean, minimum and maximum effects of varying biocrust coverage on TFVs. According to these results, a biocrust coverage of 100% causes a mean increase of TFV values by 480% (SE = 176%), ranging between 110 and 2,350% as minimum and maximum values (Extended Data Fig. 1). We combined these results with global biocrust cover data[1] (Extended Data Fig. 2) to obtain global spatially resolved information on how biocrusts affect TFVs. Our results suggest a mean global increase of TFV by ~30%, being highest on continents known to host large dust source areas, such as Australia (60%) and Africa (49%), and lowest in Europe (16%) and South America (13%; Extended Data Fig. 3).

[1]Agronomy Department, University of Almeria, Almería, Spain. [2]Multiphase Chemistry Department, Max Planck Institute for Chemistry, Mainz, Germany. [3]Institute for Atmospheric and Climate Science, ETH Zurich, Zürich, Switzerland. [4]Max Planck Institute for Meteorology, Hamburg, Germany. [5]Minerva Research Group, Max Planck Institute for Chemistry, Mainz, Germany. [6]Centro de Investigación de Colecciones Científicas de la Universidad de Almería (CECOUAL), Almería, Spain. [7]US Geological Survey, Southwest Biological Science Center, Moab, UT, USA. [8]Max Planck Institute for Chemistry, Mainz, Germany. [9]Scripps Institution of Oceanography, University of California San Diego, La Jolla, CA, USA. [10]Department of Geology and Geophysics, King Saud University, Riyadh, Saudi Arabia. [11]Leibniz Institute for Tropospheric Research, Leipzig, Germany. [12]Institute of Biology, Division of Plant Sciences, University of Graz, Graz, Austria. [13]Present address: Department of Waste, Water, Energy and Air, Canton of Zurich, Zurich, Switzerland. [14]Present address: Department of Geography, Ludwig-Maximillians University, Munich, Germany. ✉e-mail: rce959@ual.es; bettina.weber@uni-graz.at

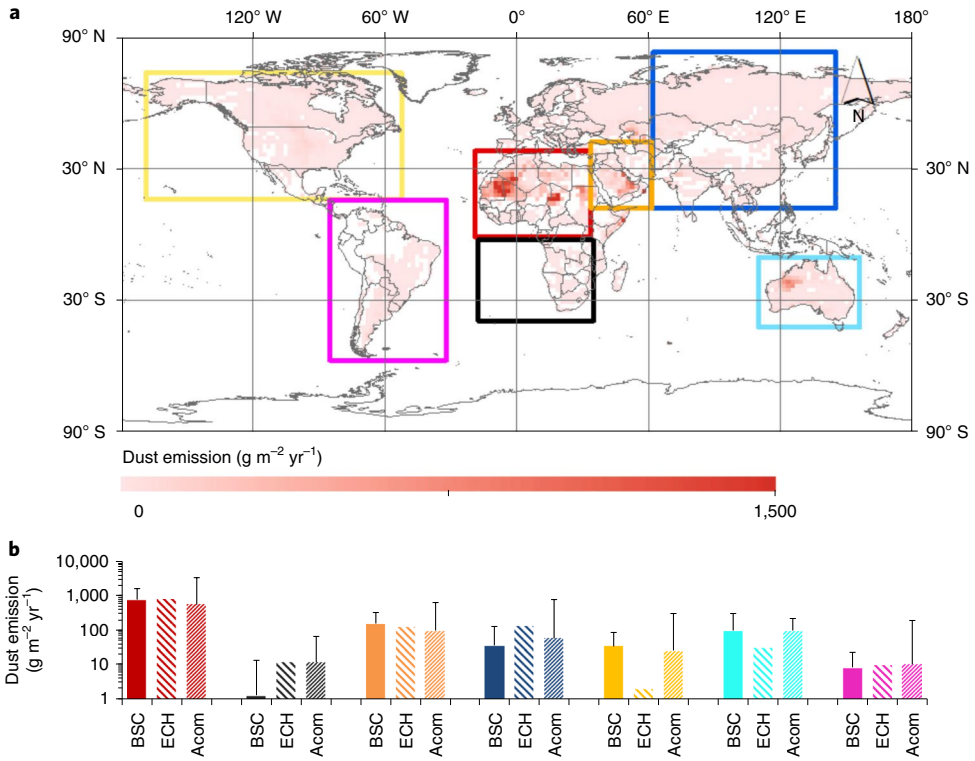

Fig. 1 | Current dust emissions obtained with the ECHAM6-HAM2-BIOCRUST model. a, Global dust emissions, considering the mean effect of biocrusts on TFV. **b**, Bar chart showing regional dust emissions obtained with the ECHAM6-HAM2-BIOCRUST model, considering the mean effect of biocrusts on TFV for the period 1990–2020. Biocrust (BSC), as compared with dust emissions obtained by the standard ECHAM6-HAM2.1 model (ECH) and the median of AeroCom (Acom) models for the different regions (indicated by different colours). Error bars in the BSC model indicate uncertainty range in our estimation (minimum and maximum effects of biocrusts on TFV) whereas error bars in Acom represent the range of values obtained by the different models considered in the AeroCom project.

These data were added to the global climate aerosol model ECHAM6-HAM2[26] with modifications of ref. [27] (ECHAM6-HAM2.1) to explicitly analyse the spatially variable effect of biocrusts on the global dust cycle. This resulted in the new model version ECHAM6-HAM2-BIOCRUST (Methods). Using this approach, we obtained an estimate of global dust emissions amounting to ~1,200 Tg yr^{-1} (Fig. 1 and Supplementary Table 2) when a mean or maximum effect of biocrusts on TFV was considered (Fig. 1). Considering a minimum biocrust effect on TFV resulted in a higher emission rate of ~1,550 Tg yr^{-1} (Supplementary Table 2). Dust deposition, as composed of sedimentation and dry and wet deposition, summed to nearly identical values. The total emission and deposition values using the mean or maximum biocrust effects were comparable to the results of the previous model version ECHAM6-HAM2.1 (931 and 945 Tg yr^{-1}, respectively; Fig. 1 and Supplementary Table 3)[27]. In this approach, biocrust effects had not been explicitly considered but were included indirectly by fitting model outputs to the observed data (see Methods for further details). Observed minor differences between our model and the previous study are based mainly on regional variations caused by biocrust presence in some potential dust source regions, such as southern Africa and the main deserts in Asia. The results are also well within the range of dust emission estimates obtained by the global dust model intercomparison project AeroCom (514–4,313 Tg yr^{-1}) (ref. [28]), presenting the state of the art in modelling of global aerosols.

Biocrust effects on current dust cycle

We then estimated the global biocrust effect on dust cycling by analysing the differences between ECHAM6-HAM2-BIOCRUST and an additional simulation after a complete removal of biocrusts (ECHAM6-HAM2-NO BIOCRUST). According to these modelling results, removal of biocrusts would cause an additional mean emission of ~700 Tg yr^{-1} (minimum biocrust effect on TFV: ~350 Tg yr^{-1}; maximum effect of biocrusts on TFV: ~700 Tg yr^{-1}) of dust, corresponding to a significant increase of ~60% (~30 to ~60%) as compared to the current value (Fig. 2a; Supplementary Table 4). This biocrust effect is particularly relevant from the west coast of North Africa, over the Middle East, Central and South Asia, to China (along the so-called dust belt) and in the main deserts of Australia, the western United States, South America and Asia. The increase of dust emissions upon biocrust removal entails a significant increase of global dust deposition that occurs mostly near dust source regions and along the main dust transport paths from these source regions (Fig. 2b). Continental dust deposition would increase by ~450 Tg yr^{-1} (~200 to ~450 Tg yr^{-1}), corresponding to an increase of ~40% (~20 to ~40%) compared to when biocrusts are present (Supplementary Table 4). Biocrust effects on continental deposition are most prominent in the biocrust-dominated areas of Africa, Asia and Australia (Supplementary Table 4), but their influence extends to remote regions in Europe, the United States and South America (Fig. 2b). Over the oceans and water bodies, biocrust removal would cause dust deposition to increase by ~250 Tg yr^{-1} (~150 to ~250 Tg yr^{-1}; Supplementary Table 5), corresponding to ~55% (~20 to ~55%) of the current values. This increased marine dust deposition would occur mainly in the form of sedimentation and wet deposition and be particularly relevant in the Indian, Pacific and Atlantic oceans (Extended Data Fig. 4 and Supplementary Table 5).

As dust also carries nutrients, source regions are depleted and deposition areas enriched[20,21,29]. Some terrestrial ecosystems within

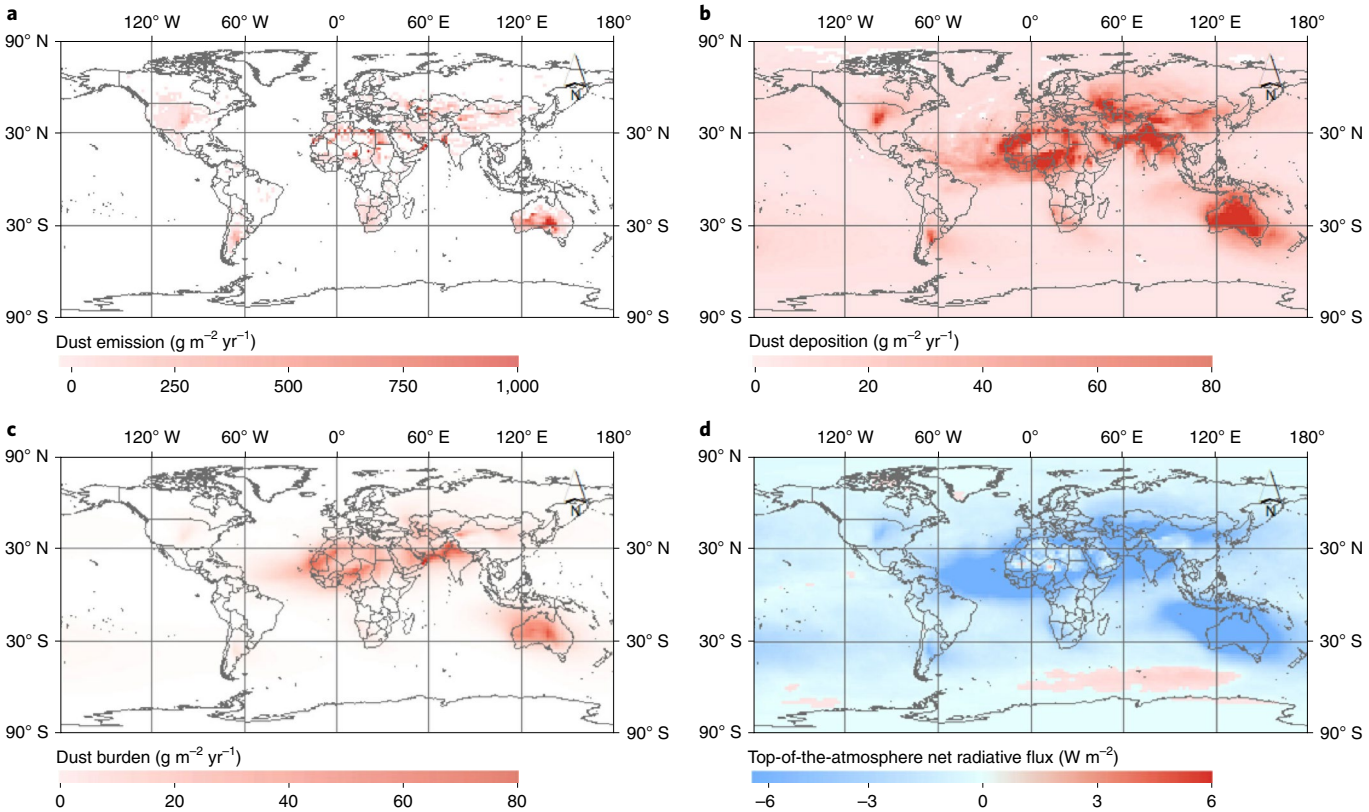

Fig. 2 | Impact of biocrusts on current global dust cycling and aerosol radiative effect. a–d, Hypothetical change of total annual dust emission (**a**), total annual dust deposition (**b**), mean annual atmospheric dust burden (**c**) and mean aerosol net radiative effect at the top of the atmosphere (**d**) upon complete removal of biocrusts. All calculations refer to mean annual values for the period 1990–2020 and are based on the mean effects of biocrusts on TFV. Individual maps showing biocrust effects on dust deposition by sedimentation, wet deposition and dry deposition are presented in Extended Data Fig. 4, and individual maps showing biocrust effects on short-wave and long-wave radiative forcing at the top of the atmosphere are shown in Extended Data Fig. 6.

the affected regions, such as the semiarid desert margins in Africa and Australia, old-growth forests within the southeastern United States, and the Amazon and Congo basins are strongly influenced by dust-borne nutrient additions[20]. It has been demonstrated that the reservoirs of soil phosphorus (P) in the Amazonian rainforest are continually depleted through plant growth and then replenished by dust-borne P input from northern Africa[15,20]. Assuming a mean P concentration of 720 ppm in dust[29], the P input in the Amazonian rainforest would be ~7 g ha^{-1} yr^{-1} higher without biocrusts, corresponding to ~100% of the estimated annual dust-borne P influx over the Amazonian basin[15]. Thus, biocrusts may indirectly affect the long-term productivity and equilibrium of the Amazonian rainforest, described as a tipping element in the Earth system[30]. However, the uncertainty inherent in these values[28] needs to be considered. Contrastingly, oligotrophic oceans and high-elevation lakes are negatively affected by dust and the accompanying nutrient input, which can damage coral reefs[31] and increase harmful algal and bacterial blooms[32].

Biocrust effects on atmospheric dust load and radiation

Because biocrust covers reduce dust emissions, they also significantly lower the mean global atmospheric dust burden by ~8.5 Tg (~5.0 to ~8.5 Tg), corresponding to a decrease by ~55% (Fig. 2c and Supplementary Table 6). This also significantly affects the overall aerosol optical depth (AOD), causing a decrease of ~20% (~5 to ~20%; Extended Data Fig. 5). Without biocrusts, both the dust burden and AOD will strongly increase near dust source areas currently densely covered by biocrusts (Extended Data Fig. 2), such as the main deserts of northern Africa, the Arabian Peninsula, India and Australia and along their downwind atmospheric pathways (Fig. 2c and Extended Data Fig. 5). Several studies have also described a potential effect of dust on human health, potentially aggravating cardiovascular and respiratory diseases[33].

As dust particles interfere with both incoming short-wave and outgoing long-wave radiation, biocrusts significantly modify the global radiation budget by preventing dust emissions. Overall net aerosol radiative effects at the top of the atmosphere, which are estimated at −3.5 W m^{-2}, would decrease by up to 0.48 W m^{-2} (0.02 to 0.48 W m^{-2}; Fig. 2d and Supplementary Table 6) upon the removal of biocrusts. These effects are based mainly on short-wave contributions causing a decrease of 0.58 W m^{-2} (0.04 to 0.58 W m^{-2}), whereas long-wave contributions cause an increase of 0.10 W m^{-2} (0.02 to 0.10 W m^{-2}; Fig. 2d, Extended Data Fig. 6 and Supplementary Table 6). The biocrust influence on the overall radiative effect of dust is similar to the total direct forcing of anthropogenic aerosols (-0.35 ± 0.5 W m^{-2}) (ref. [34]) and three times larger than the effect attributed to dust emissions produced by past land-use change[27]. Thus, we consider biocrusts to be relevant in regulating the effect of dust on regional climate processes, both close to the source areas and in the global solar radiation budget[16]. However, these results should be considered with caution, as recent studies suggest that the dust found in the atmosphere is substantially coarser than assumed in current global climate models, thus having a smaller cooling or potentially even a warming effect over bright land surfaces, contrasting the assumptions of previous models[16].

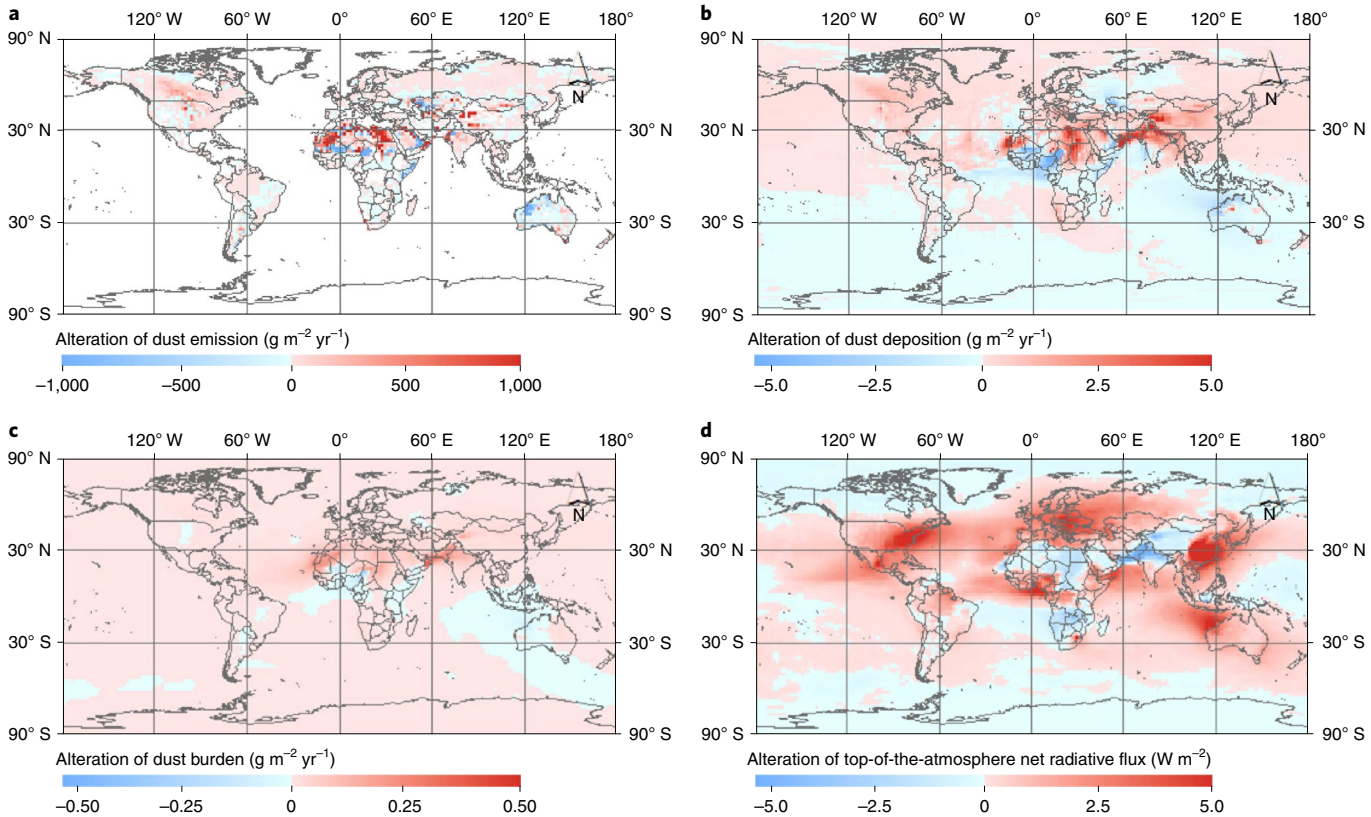

Fig. 3 | Effect of global change and the induced biocrust cover loss estimated by 2070 on future dust cycling. a–d, Change in future total annual dust emission (**a**), total annual dust deposition (**b**), mean annual atmospheric dust burden (**c**) and mean annual aerosol net radiative effect at the top of the atmosphere (**d**). Data calculated according to RCP 2.6. Individual maps showing biocrust effects on dust cycling according to RCP 4.5 and RCP 8.5 are shown in Extended Data Figs. 7 and 8, respectively.

The effects of future biocrust loss

Biocrusts have been shown to be sensitive to changes in environmental parameters and land-use intensification[35]. On the basis of the climate and land-use projections presented by the Fifth Assessment Report of the Intergovernmental Panel on Climate Change (IPCC)[14], predicting increased temperatures, modified precipitation regimes and intensified land use in drylands for the upcoming decades, we analysed the response of biocrust covers to these changes in a former study[1]. According to an analysis of the different scenarios (representative concentration pathways; RCPs), the biocrust cover will be reduced by ~25 to 40% by the year 2070[1]. Under these future conditions, global dust emission and deposition would increase by ~5 to 15%, depending on the scenario used (Fig. 3, Extended Data Figs. 7 and 8 and Supplementary Tables 7 and 8). Strong increases in dust emissions are to be expected in some regions of northern Africa and the Middle East, whereas dust emissions may decrease in other parts of the Sahel, Asia and Australia due to interactions between increased vegetation coverage and a modified wind regime (Fig. 3a). Higher dust emissions may cause a strong increase in dust deposition along the dust belt, which will extend to major parts of the Northern Hemisphere, whereas it will be locally reduced around dust source regions in the Sahel and Australia (Fig. 3b). These results are in contrast to the generally expected decrease in global dust production due to the Sahel greening by CO_2 fertilization[36]. Our model reveals that this intensification of the future dust cycle is driven mainly by the anthropogenically induced biocrust loss (Extended Data Fig. 9). In addition, indirect effects of amplified warming over northern Africa, causing shorter atmospheric residence times and modified dust transport routes, were suggested to reduce the dust burden and AOD by the end of the century[37]. However, according to our model, the loss of biocrusts will counteract this effect (Extended Data Fig. 9), causing an increase of the dust burden by up to 16% (Fig. 3c) with a reduction of the global radiation budget by around 0.12 to 0.22 W m^{-2}, depending on the model parameterization and RCP used (Fig. 3d and Extended Data Figs. 7 and 8). Moreover, according to ref. [38], increased dust over the Sahel will probably trigger changes in atmospheric circulation, which may affect cyclone activity in the tropical Atlantic[39] and could result in multiple regional climate alterations. As the current analyses are based on data of varying spatial resolution and some small-scale parameters influencing dust emissions (as, for example, small-scale atmospheric and geographical features) are lacking, global dust simulations generally still comprise significant uncertainties[16,37]. These need to be tackled, once more-detailed high-quality baseline data are available.

Figure 4 summarizes the importance of biocrusts in the current and future dust cycle, which up to now has been overlooked in Earth system models. Stabilizing the soil surface, biocrusts currently prevent the emission and redistribution of ~700 Tg of dust per year, reducing the total atmospheric dust load by ~55% and affecting the radiative balance. This protective effect of biocrusts will be reduced in the future because of an expected biocrust cover loss, which could override the generally expected decrease in global dust production due to the Sahel greening by CO_2 fertilization. The increased dust cycling will play an important role in land and ocean productivity and atmospheric radiative forcing, with direct implications on the future climate near major source regions. As the transported dust carries microorganisms and potentially introduces new

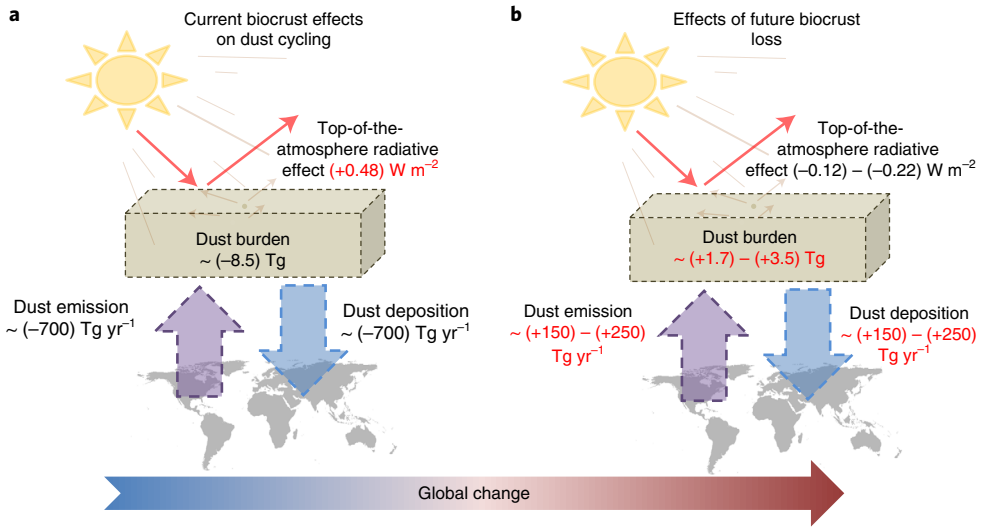

Fig. 4 | Effect of biocrusts on current global dust cycling and future changes with expected biocrust cover loss. a, Current effect of biocrusts on mean annual global dust emission, dust deposition, atmospheric dust burden and net radiative effect at the top of the atmosphere (period 1990–2020). **b**, Expected effects of anthropogenically induced biocrust cover loss by 2070 on future mean annual global dust emission, dust deposition, atmospheric dust burden and net radiative effect at the top of the atmosphere (calculated according to RCP 2.6 and RCP 8.5). Increases (decreases) of values are shown in red (black) letters.

pathogens, it also poses a potential risk for the local microbiome and human health[40]. Besides this overall reduction in biocrust coverage, climate manipulation experiments showed that disturbance, warming and changes in precipitation patterns may have dramatic effects on biocrust community composition, with likely alterations towards early successional cyanobacteria-dominated biocrusts[35]. As cyanobacteria-dominated biocrusts have a lower soil-stabilizing effect[41] and tend to have a darker surface colouration, this may further reinforce the dust production and affect the radiative balance[42].

Overall, our results suggest that studies analysing dust cycling and its effects on Earth system functioning and human health need to incorporate all the interrelated effects of biocrusts, which up to now have been overlooked. Increased data availability on the soil-stabilizing role of biocrusts will help to confine biocrust effects and reduce uncertainties in current and future estimates. Biocrusts probably played a substantial role in soil and dust formation already during Precambrian times, when they formed the only existing terrestrial ecosystem[43], and our results suggest that they are also relevant in dust cycling under current and future conditions. We think our study could help to reduce the current uncertainty regarding some of the most important knowledge gaps identified in the IPCC Special Report on Climate Change and Land, such as the climate change impacts on dust- and sandstorm activity and the future interactions between climate and desertification[44].

Online content

Any methods, additional references, Nature Research reporting summaries, source data, extended data, supplementary information, acknowledgements, peer review information; details of author contributions and competing interests; and statements of data and code availability are available at https://doi.org/10.1038/s41561-022-00942-1.

Received: 2 March 2021; Accepted: 30 March 2022;
Published online: 16 May 2022

References

1. Rodriguez-Caballero, E. et al. Dryland photoautotrophic soil surface communities endangered by global change. *Nat. Geosci.* **11**, 185–189 (2018).
2. Weber, B., Belnap, J. & Büdel, B. *Biological Soil Crusts: An Organizing Principle in Drylands* 1st edn (Springer, 2016).
3. Elbert, W. et al. Contribution of cryptogamic covers to the global cycles of carbon and nitrogen. *Nat. Geosci.* **5**, 459–462 (2012).
4. Maier, S. et al. Photoautotrophic organisms control microbial abundance, diversity, and physiology in different types of biological soil crusts. *ISME J.* **12**, 1032–1046 (2018).
5. Havrilla, C. A. et al. Towards a predictive framework for biocrust mediation of plant performance: a meta-analysis. *J. Ecol.* **107**, 2789–2807 (2019).
6. Eldridge, D. J. et al. The pervasive and multifaceted influence of biocrusts on water in the world's drylands. *Glob. Change Biol.* **26**, 6003–6014 (2020).
7. Meusel, H. et al. Emission of nitrous acid from soil and biological soil crusts represents an important source of HONO in the remote atmosphere in Cyprus. *Atmos. Chem. Phys.* **18**, 799–813 (2018).
8. Weber, B. et al. Biological soil crusts accelerate the nitrogen cycle through large NO and HONO emissions in drylands. *Proc. Natl Acad. Sci. USA* **112**, 15384–15389 (2015).
9. Andreae, M. O. & Crutzen, P. J. Atmospheric aerosols: biogeochemical sources and role in atmospheric chemistry. *Science* **276**, 1052–1058 (1997).
10. Olsson, P. Q. & Benner, R. L. Atmospheric chemistry and physics: from air pollution to climate change. *J. Am. Chem. Soc.* **121**, 1423–1423 (1999).
11. Rossi, F. & De Philippis, R. Role of cyanobacterial exopolysaccharides in phototrophic biofilms and in complex microbial mats. *Life* **5**, 1218–1238 (2015).
12. Pointing, S. B. & Belnap, J. Disturbance to desert soil ecosystems contributes to dust-mediated impacts at regional scales. *Biodivers. Conserv.* **23**, 1659–1667 (2014).
13. Penner, J. E. Soot, sulfate, dust and the climate—three ways through the fog. *Nature* **570**, 158–159 (2019).
14. IPCC *Climate Change 2013: The Physical Science Basis* (eds Stocker, T. F. et al.) (Cambridge Univ. Press, 2013).
15. Prospero, J. M. et al. Characterizing and quantifying African dust transport and deposition to South America: implications for the phosphorus budget in the Amazon basin. *Glob. Biogeochem. Cycles* **34**, e2020GB006536 (2020).
16. Kok, J. F., Ward, D. S., Mahowald, N. M. & Evan, A. T. Global and regional importance of the direct dust–climate feedback. *Nat. Commun.* **9**, 241 (2018).
17. Morris, C. E. et al. Bioprecipitation: a feedback cycle linking Earth history, ecosystem dynamics and land use through biological ice nucleators in the atmosphere. *Glob. Change Biol.* **20**, 341–351 (2014).
18. DeMott, P. J. et al. Predicting global atmospheric ice nuclei distributions and their impacts on climate. *Proc. Natl Acad. Sci. USA* **107**, 11217–11222 (2010).
19. Klingmüller, K., Lelieveld, J., Karydis, V. A. & Stenchikov, G. L. Direct radiative effect of dust–pollution interactions. *Atmos. Chem. Phys.* **19**, 7397–7408 (2019).
20. Field, J. P. et al. The ecology of dust. *Front. Ecol. Environ.* **8**, 423–430 (2010).
21. Okin, G. S., Mahowald, N., Chadwick, O. A. & Artaxo, P. Impact of desert dust on the biogeochemistry of phosphorus in terrestrial ecosystems. *Glob. Biogeochem. Cycles* **18**, GB2005 (2004).

22. Pabortsava, K. et al. Carbon sequestration in the deep Atlantic enhanced by Saharan dust. *Nat. Geosci.* **10**, 189–194 (2017).
23. Painter, T. H. et al. Impact of disturbed desert soils on duration of mountain snow cover. *Geophys. Res. Lett.* **34**, L12502 (2007).
24. Belnap, J., Phillips, S. L., Herrick, J. E. & Johansen, J. R. Wind erodibility of soils at Fort Irwin, California (Mojave Desert), USA, before and after trampling disturbance: implications for land management. *Earth Surf. Process. Landf.* **32**, 75–84 (2007).
25. Zhang, Y. M., Wang, H. L., Wang, X. Q., Yang, W. K. & Zhang, D. Y. The microstructure of microbiotic crust and its influence on wind erosion for a sandy soil surface in the Gurbantunggut Desert of Northwestern China. *Geoderma* **132**, 441–449 (2006).
26. Zhang, K. et al. The global aerosol–climate model ECHAM-HAM, version 2: sensitivity to improvements in process representations. *Atmos. Chem. Phys.* **12**, 8911–8949 (2012).
27. Stanelle, T., Bey, I., Raddatz, T., Reick, C. & Tegen, I. Anthropogenically induced changes in twentieth century mineral dust burden and the associated impact on radiative forcing. *J. Geophys. Res. Atmos.* **119**, 13526–13546 (2014).
28. Huneeus, N. et al. Global dust model intercomparison in AeroCom phase I. *Atmos. Chem. Phys.* **11**, 7781–7816 (2011).
29. Mahowald, N. et al. Global distribution of atmospheric phosphorus sources, concentrations and deposition rates, and anthropogenic impacts. *Glob. Biogeochem. Cycles* **22**, GB4026 (2008).
30. Lenton, T. M. et al. Tipping elements in the Earth's climate system. *Proc. Natl Acad. Sci. USA* **105**, 1786–1793 (2008).
31. Shinn, E. A. et al. African dust and the demise of Caribbean coral reefs. *Geophys. Res. Lett.* **27**, 3029–3032 (2000).
32. Westrich, J. R. et al. Saharan dust nutrients promote bloom formation in marine surface waters. *Proc. Natl Acad. Sci. USA* **113**, 5964–5969 (2016).
33. De Longueville, F., Hountondji, Y.-C., Henry, S. & Ozer, P. What do we know about effects of desert dust on air quality and human health in West Africa compared to other regions? *Sci. Total Environ.* **409**, 1–8 (2010).
34. Boucher, O. et al. in *Climate Change 2013: The Physical Science Basis* (eds Stocker, T. F. et al.) 571–658 (IPCC, Cambridge Univ. Press, 2013).
35. Ferrenberg, S., Reed, S. C. & Belnap, J. Climate change and physical disturbance cause similar community shifts in biological soil crusts. *Proc. Natl Acad. Sci. USA* **112**, 12116–12121 (2015).
36. Mahowald, N. M. et al. Change in atmospheric mineral aerosols in response to climate: last glacial period, preindustrial, modern, and doubled carbon dioxide climates. *J. Geophys. Res. Atmos.* **111**, D10202 (2006).
37. Tegen, I. & Schepanski, K. Climate feedback on aerosol emission and atmospheric concentrations. *Curr. Clim. Change Rep*. https://doi.org/10.1007/s40641-018-0086-1 (2018).
38. Albani, S. & Mahowald, N. M. Paleodust insights into dust impacts on climate. *J. Clim.* **32**, 7897–7913 (2019).
39. Pausata, F. S. R. et al. Tropical cyclone activity enhanced by Sahara greening and reduced dust emissions during the African Humid Period. *Proc. Natl Acad. Sci. USA* **114**, 6221–6226 (2017).
40. Behzad, H., Mineta, K. & Gojobori, T. Global ramifications of dust and sandstorm microbiota. *Genome Biol. Evol.* **10**, 1970–1987 (2018).
41. Belnap, J. & Gillette, D. A. Vulnerability of desert biological soil crusts to wind erosion: the influences of crust development, soil texture, and disturbance. *J. Arid Environ.* **39**, 133–142 (1998).
42. Rutherford, W. et al. Albedo feedbacks to future climate via climate change impacts on dryland biocrusts. *Sci. Rep.* **7**, 44188 (2017).
43. Beraldi-Campesi, H. & Ratallack, G. J. in *Biological Soil Crusts: An Organizing Principle in Drylands* (eds Weber, B. et al.) 37–54 (Springer, 2016).
44. Mirzabaev, A. et al. in *Special Report on Climate Change and Land* (eds Shukla, P. R. et al.) Ch. 3 (IPCC, 2019).

Methods

Parameterization of biocrust effects on dust emissions. *Biocrust effects on TFV.* Biocrust effects on TFV were assessed by compiling available literature data that include information on the TFV of soils covered by biocrusts, the TFV of the underlying bare soil, the biocrust type and cover, the treatment (potential disturbance), soil texture, precipitation and the study area. Only data comprising information on both the biocrust and the bare soil TFV could be used to calculate a biocrust TFV increase ratio, which reflects the effect of biocrusts on TFV, that is, a percentual increase of biocrust TFV compared with the TFV of the underlying reference soil (Supplementary Table 1a,b). As shown in Supplementary Table 1c, there are by far more data available where biocrust TFV but not the underlying soil TFV has been measured. Here, it becomes clear that the biocrust TFV data used in the study are rather conservative. In fact, the mean TFV of the data that were used in the study is considerably lower (298 cm s^{-1}) than that of the biocrust data that could not be used (due to the missing TFV data of the underlying soil; 729 cm s^{-1}; see Extended Data Fig. 1a).

We first used the experimental data provided by ref. [25], where the effect of different biocrust cover values on the TFV was investigated to determine the overall function ruling the relationship between the factors[25]. This analysis demonstrated that with increasing biocrust cover values, the biocrust effect on TFV increased in an exponential manner, according to equation (1) (Extended Data Fig. 1b).

$$\text{TFV increase ratio} = e^{a \times \text{biocrusts cover}} \quad (1)$$

where TFV increase ratio (in %) is the rate of TFV alteration with biocrust cover changes compared with the TFV of the underlying reference soil, e is Euler's number and a is a constant describing the rate of TFV alteration with increasing biocrust coverage. The function was also corroborated by an additional study[45] that analysed restored biocrusts and non-natural communities (Extended Data Fig. 1b).

As most experimental datasets corresponded to plots with 100% coverage (Supplementary Table 1), in a second step, we applied this exponential function to all the available data showing the effect of biocrusts of 100% coverage on TFV to parameterize a minimum, mean and maximum model (Extended Data Fig. 1b). To do this, a values were calculated separately for the three different models by solving equation (1) to fit the average (TFV increase at 100% coverage = 479% and $a = 0.0157$), maximum (TFV increase at 100% coverage = 2,350% and $a = 0.0316$) and minimum (TFV increase at 100% coverage = 114% and $a = 0.0013$) values of increase in TFV on soils with 100% biocrust coverage, as shown in Supplementary Table 1 and Extended Data Fig. 1. With this combined approach, we could estimate the biocrust effect on TFV over the complete range of biocrust cover values and account for the uncertainty included in the modelling approach. The mean model has been calculated on the basis of the geometric mean, which is less affected by extreme values and more conservative than the arithmetic mean.

Global biocrust coverage. Global biocrust spatial distribution and cover data were adopted from a previous study, where the maximum entropy method was applied to define a set of 18 parameters and environmental variables describing the spatial distribution of biocrusts on a global scale[1]. This layer was resampled to the spherical harmonics T63 resolution according to the horizontal spatial resolution of ECHAM-HAM2.1 (approximately 210 km × 210 km at the Equator; Extended Data Fig. 2) to be used in the dust modelling approach.

Modelling of biocrust effects in the model ECHAM6-HAM2.1. *Dust emission model.* Dust emissions were modelled using the global climate aerosol model ECHAM6-HAM2[26] and the dust source scheme of ref. [46], including improvements of ref. [27], which benefit from the online coupling between the atmospheric and the land component (JSBACH) in the ECHAM6 global climate model (ECHAM6-HAM2.1). The model simulates dust emissions, taking into account the vegetation type, cover and seasonality, agricultural conservation practices, soil particle size distribution, snow cover, soil moisture and surface wind speed. Each grid cell is divided into a bare and a vegetated fraction. The vegetated fraction is further divided into 11 plant functional types. Emissions occur only from bare surface areas and the gaps between low-stature plant functional types (natural shrubs, grass, tundra, swamp, crop and pasture) when wind velocity rises above the TFV of the soil surface and if other criteria are satisfied (for example, soil dryness, absence of snow cover). In each grid cell where dust emission could occur, the emission flux is calculated separately for 192 dust size classes (0.2–1,300 µm]. To do so, an individual TFV value as well as a ratio between vertical and horizontal dust flux is prescribed for each of the dust size classes following the process described by ref. [47]. Finally, the vertical emission fluxes are integrated over the 192 dust size classes and attributed to two aerosols modes: the insoluble accumulation (mass mean radius = 0.37 µm) and the coarse mode (mass mean radius = 1.75 µm; standard deviation (sigma) = 1.59; see ref. [46] for more details). The super-coarse mode is neglected because of its short lifetime[48,49]. The particle size distribution of each grid cell is obtained from the soil textural classes defined in the soil map of the world by the Food and Agriculture Organization/United Nations Educational, Scientific, and Cultural Organization[50] as described in ref. [46].

Development of ECHAM6-HAM2-BIOCRUST. The ECHAM6-HAM2.1 model was modified to explicitly account for the effect of biocrusts on wind erosion and dust emissions (ECHAM6-HAM2-BIOCRUST). To do that, we applied the exponential models, which describe the mean, maximum and minimum rate of TFV alteration, related to biocrust cover changes (section Biocrust effect on TFV), to the resampled biocrust cover map (Extended Data Fig. 2). Doing this, we obtained spatially distributed values of the mean, maximum, and minimum rate of TFV increase, resulting from biocrust presence data (Extended Data Fig. 3).

Simulation set-up. We performed five simulations for the period 1990–2020 at a resolution of 63 horizontal (T63; ~210 km at the Equator) and 31 vertical (L31) levels. The set-up was as follows: (1) a simulation with the standard version of ECHAM6-HAM2.1, which implicitly considers biocrust effects on dust emissions; (2) three different simulations with mean, minimum and maximum TFV values determined for biocrusts (see section Biocrust effect on TFV; ECHAM6-HAM2-BIOCRUST); (3) an additional simulation using ECHAM6-HAM2-BIOCRUST not accounting for the effect of biocrusts on TFV (ECHAM6-HAM2-NO BIOCRUST). The standard version of ECHAM6-HAM2.1 applies a global correction factor of 0.9 to the TFV to fit the obtained dust emissions to the observed data. By setting the correction factor to a value that best represents the observed data, the model indirectly considers the biocrust effect (although the scientists were not aware of the existence and relevance of biocrusts). For simulations described under (2) and (3), the global correction factor was set to 0.80 after preliminary sensitivity simulations with different values (0.9; 0.85; 0.80). By doing this, the resulting values better represent the overall dust emission rates obtained by ref. [27], which have been comprehensively evaluated against observations. Doing this, we were able to analyse explicitly the spatially variable effect of biocrusts on the global dust cycle.

Biocrust effects on dust emission, dust deposition, dust load and radiative balance. In a first step, we compared regional averages of mean annual dust emission values obtained by ECHAM6-HAM2-BIOCRUST with these obtained by ECHAM6-HAM2.1 and with the data reported by the AeroCom initiative[27,28] to evaluate the ability of the new model to characterize the effect of biocrusts on global dust sources and distribution. Then, we estimated the mean biocrust effect as well as uncertainty ranges (minimum and maximum biocrust effect) on dust emissions, dust sedimentation, dust wet and dry deposition, dust burden, AOD and net aerosol radiative effects at the top of the atmosphere. We did this by calculating the difference between the mean annual values of the 30-year simulations of ECHAM6-HAM2-BIOCRUST and ECHAM6-HAM2-NO BIOCRUST. Significant differences between global annual values obtained from the different parameterizations of ECHAM6-HAM2-BIOCRUST (mean, maximum and minimum biocrust effect on TFV) and ECHAM6-HAM2-NO BIOCRUST were identified by applying a one-way ANOVA and a Tukey´s post hoc test. Before the ANOVA, all data were tested for normality assumptions. Finally, we applied an additional one-way ANOVA to identify whether differences between ECHAM6-HAM2-BIOCRUST and ECHAM6-HAM2-NO BIOCRUST simulations were significant in each pixel. Only significant changes are shown in the maps.

Biocrust effects on future dust emissions. Recent studies demonstrated that the global biocrust coverage will decrease by 25–40% by 2070 due to anthropogenically caused climate change and land-use intensification[1]. The effect of the predicted biocrust cover loss on future dust emissions was calculated according to three different RCPs defined in the Fifth Assessment Report of the IPCC (RCPs 2.6, 4.5 and 8.5), reflecting an increase of 2.6, 4.5, and 8.5 W m^{-2} by the year 2100 relative to pre-industrial values, as determined by the Coupled Model Intercomparison Project 5[14]. For this, we first applied the exponential models, which describe the average, maximum and minimum rate of TFV increase with increasing biocrust cover (Extended Data Fig. 1), to the future biocrust map by ref. [1], predicting the biocrust cover by 2070. Before this, the map had been resampled to the spatial resolution of the model (section Global biocrust coverage). Using the resulting maps and ECHAM6-HAM2-BIOCRUST, we simulated dust emissions for the period 2055–2085 for each RCP, as described in section Development of ECHAM6-HAM2-BIOCRUST. Moreover, we simulated dust deposition, dust sedimentation, total dust load and radiative balance at the top of the atmosphere for the three different RCPs using future climate, future vegetation and current biocrust distribution. Then we estimated the effect of biocrust cover loss on future dust cycling as the difference between simulations (future simulation considering predicted biocrust coverage by 2070 and future simulation considering current biocrust distribution). By doing this, we were able to distinguish between the effects of future climate conditions and vegetation cover change as opposed to biocrust cover loss on the future dust cycling. Significant differences between the future simulations considering the biocrust coverage predicted for 2070 and the current biocrust distribution were identified by applying a one-way ANOVA and a Tukey´s post hoc test. Before the ANOVA, all data were tested for normality assumptions.

Data availability

Raster layers describing the biocrust effect on TFV for current and future conditions are publicly available at https://doi.org/10.17617/3.F6ZSUP.

Code availability

The ECHAM6-HAM2 BIOCRUSTS code is an extension to the ECHAM6–HAMMOZ code, which is maintained and made available to the scientific community at https://redmine.hammoz.ethz.ch/ (HAMMOZ consortium, 2017). The availability is regulated under the HAMMOZ Software Licence Agreement that can be downloaded from https://redmine.hammoz.ethz.ch/attachments/download/291/License_ECHAM-HAMMOZ_June2012.pdf.

References

45. Zhang, Z., Dong, Z., Zhao, A., Yuan, W. & Han, L. The effect of restored microbiotic crusts on erosion of soil from a desert area in China. *J. Arid Environ.* **72**, 710–721 (2008).
46. Tegen, I. et al. Impact of vegetation and preferential source areas on global dust aerosol: results from a model study. *J. Geophys. Res. Atmos.* **107**, 4576 (2002).
47. Marticorena, B. et al. Modeling the atmospheric dust cycle: 2. simulation of Saharan dust sources. *J. Geophys. Res. Atmos.* **102**, 4387–4404 (1997).
48. Cheng, T., Peng, Y., Feichter, J. & Tegen, I. An improvement on the dust emission scheme in the global aerosol–climate model ECHAM5-HAM. *Atmos. Chem. Phys.* **8**, 1105–1117 (2008).
49. Stier, P. et al. The aerosol–climate model ECHAM5-HAM. *Atmos. Chem. Phys.* **5**, 1125–1156 (2005).
50. Zobler, L. *Global Soil Types, 1-Degree Grid* (OCNL DAAC, 1999); https://doi.org/10.3334/ORNLDAAC/418

Acknowledgements

We thank the scientific community within the Max Planck Institute for Chemistry for the support, stimulating atmosphere and many inspiring discussions. This work is dedicated to Paul J. Crutzen, whose curiosity across scientific borders and active engagement in topics of global environmental concerns has inspired our work. We also thank C. Pöhlker, A. Solé and S. Chamizo for critically reading the manuscript. This work was supported by the Max Planck Society and the Paul Crutzen Nobel Laureate Fellowship (awarded to E.R.-C. and B.W.). E.R.-C. was also supported by the GLOB-CRUST project (EMERGIA20_0033) founded by the Consejeria de transformacion economica, industria, Conocimiento y universidades, the Ramon y Cajal fellowship (RYC2020-030762-I) and the REBIOARID Project (2018-101921-B-I00) founded by FEDER/Ministerio de Ciencia e Inovacion-Agencia estatal de investigacion, and the BIOCOST project (Conservación debiocostras como estrategia de adaptación al cambio climático: alineando avances científicos con la gestión y sociedad) supported by the Biodiversity Foundation of the Ministry for the Ecological Transition and the Demographic Challenge. J.B. has been supported by the USGS Land Use Change and Ecosystems programmes. Any use of trade, product or firm names is for descriptive purposes only and does not imply endorsement by the US Government. We gratefully acknowledge support by Deutsches Klimarechenzentrum (DKRZ), where the simulations have been performed.

Author contributions

E.R.-C., B.W., T.S., S.E. and C.H.R. designed the study. E.R.-C. and B.W. analysed the data. E.R.-C., T.S., S.E. and C.H.R. developed the models. E.R.-C., B.W., U.P., Y.Ch. and H.S. wrote the paper, and all authors contributed to interpreting the data.

Funding

Open access funding provided by Max Planck Society.

Competing interests

The authors declare no competing interests.

Additional information

Extended data is available for this paper at https://doi.org/10.1038/s41561-022-00942-1.

Supplementary information The online version contains supplementary material available at https://doi.org/10.1038/s41561-022-00942-1.

Correspondence and requests for materials should be addressed to E. Rodriguez-Caballero or B. Weber.

Peer review information *Nature Geoscience* thanks the anonymous reviewers for their contribution to the peer review of this work. Primary Handling Editors: Tamara Goldin and Xujia Jiang, in collaboration with the *Nature Geoscience* team.

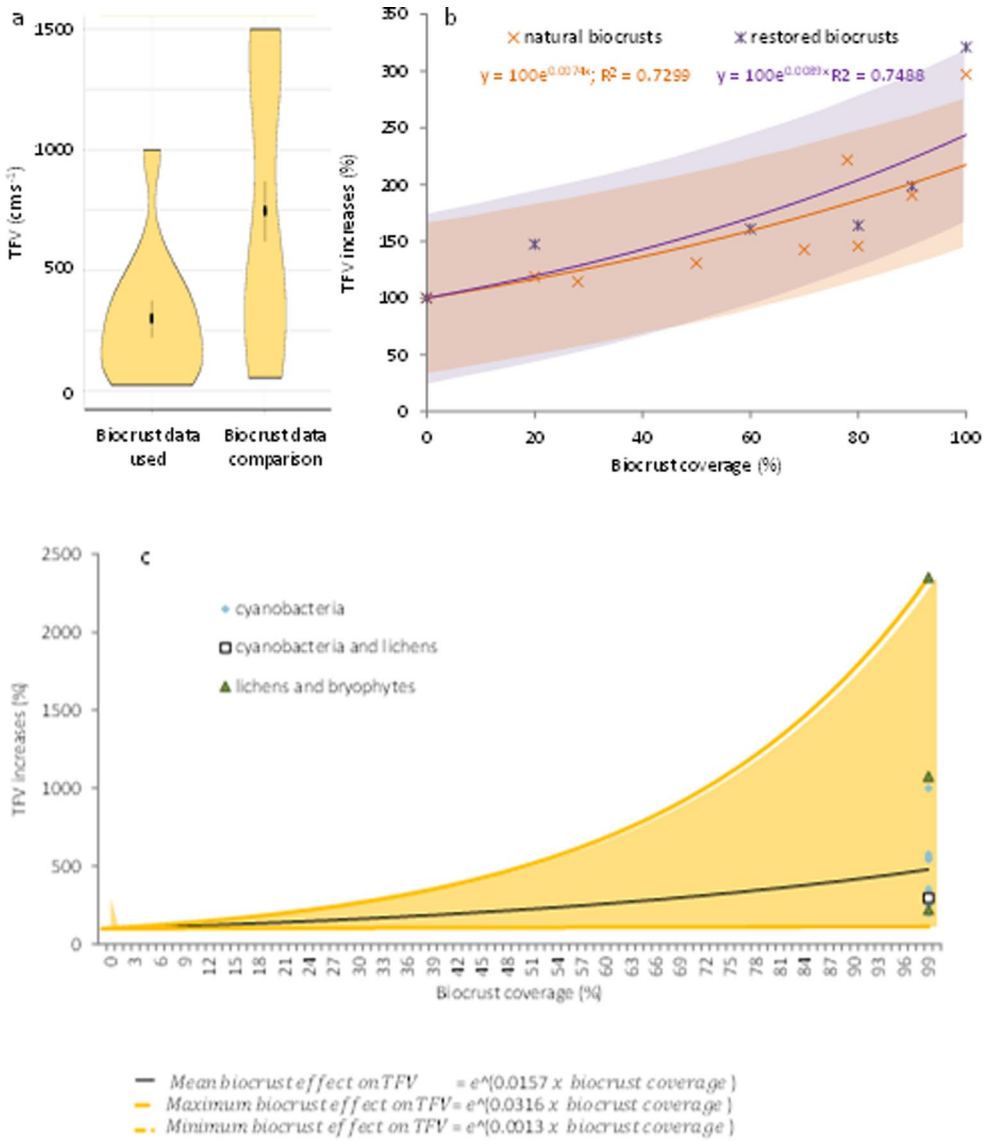

Extended Data Fig. 1 | Impact of biocrusts on threshold friction velocity. (a) Threshold friction velocity values of biocrust data that were used in the study as compared to values which could not be used (due to missing values of reference soils; see Supplementary Table 1b,c). Black dot and line indicate the mean and standard error. **(b)** Exponential fits (lines) and 95% confidence intervals (shaded areas) between coverage of natural[25] and restored biocrusts[45] and the biocrust effect on Threshold Friction Velocity (TFV; in %); and **(c)** Exponential model describing biocrust coverage effects on Threshold Friction Velocity (TFV; in %). Three different models were developed, considering mean (geometric mean), maximum, and minimum effects on biocrust TFV (see Supplementary Table 1b).

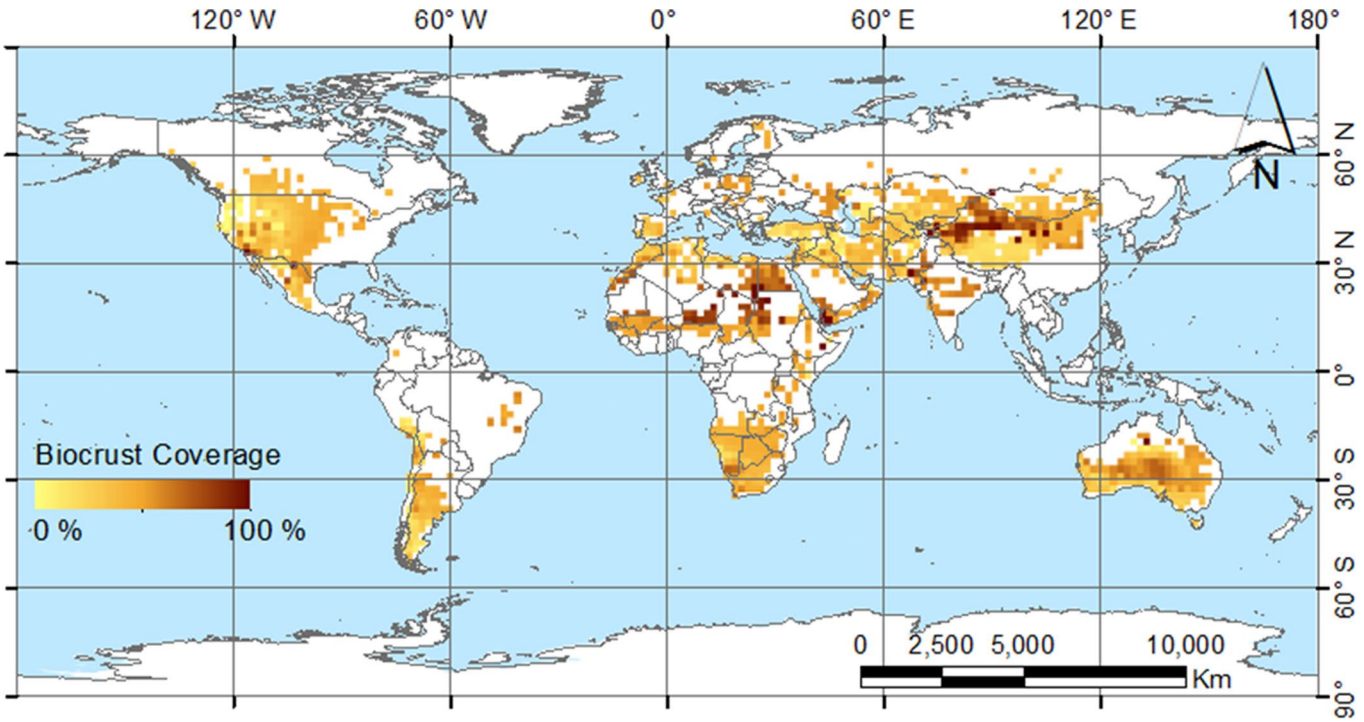

Extended Data Fig. 2 | Global biocrust coverage. Biocrust cover map (in %) obtained from[1] and resampled to the spatial resolution needed by the ECHAM6-HAM2-BIOCRUST model (spherical harmonics T63; spatial resolution approximately 210 km × 210 km at the equator).

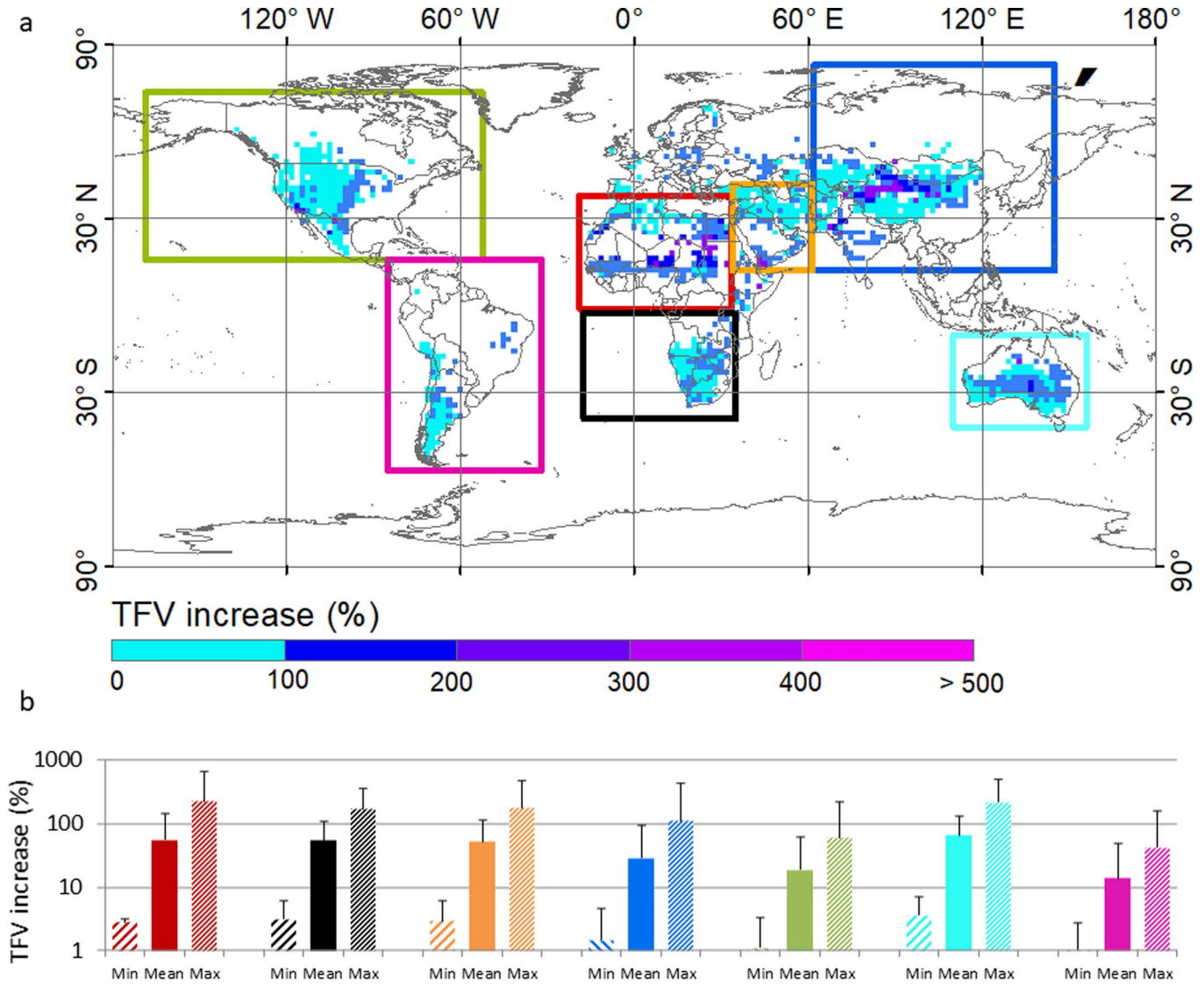

Extended Data Fig. 3 | Impact of biocrusts on threshold friction velocity (TFV). (a) Global map of TFV increase as consequence of biocrust effects on soil surface stability, considering the mean model shown in Supplementary Fig. 1. **(b)** Bar charts showing average ± standard deviation of biocrust induced increase in TFV by regions for the ECHAM6-HAM2-BIOCRUST model, accounting for mean (Mean) maximum (Max) and minimum (Min) effect of biocrusts on TFV.

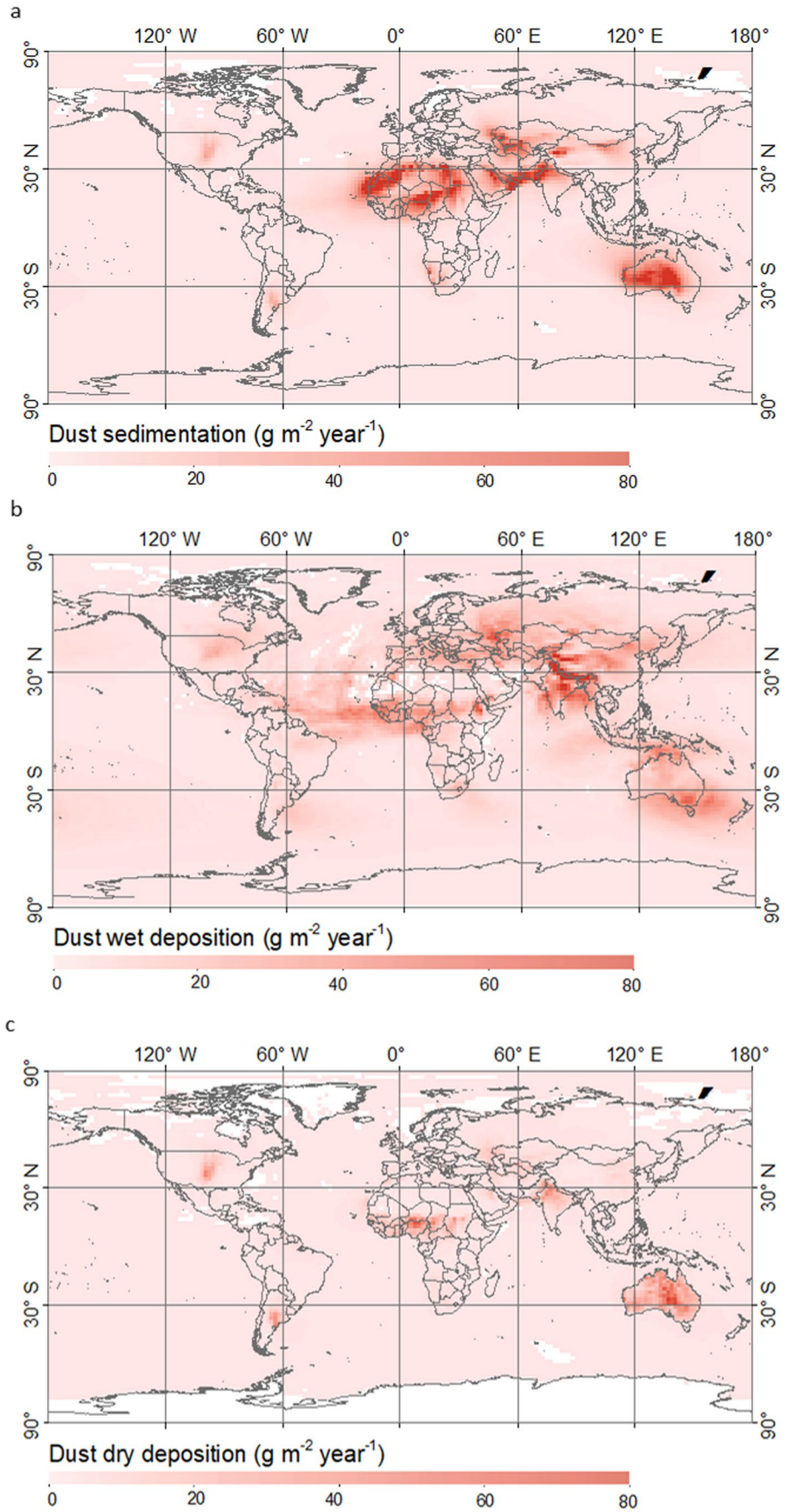

Extended Data Fig. 4 | Impact of biocrusts on mean annual dust deposition [in g m^{-2} a^{-1}]. Hypothetical change of **(a)** dust deposition by sedimentation, **(b)** wet deposition, and **(c)** dry deposition upon complete removal of biocrusts. For calculations, mean effects of biocrusts on threshold friction velocity (TFV) were considered.

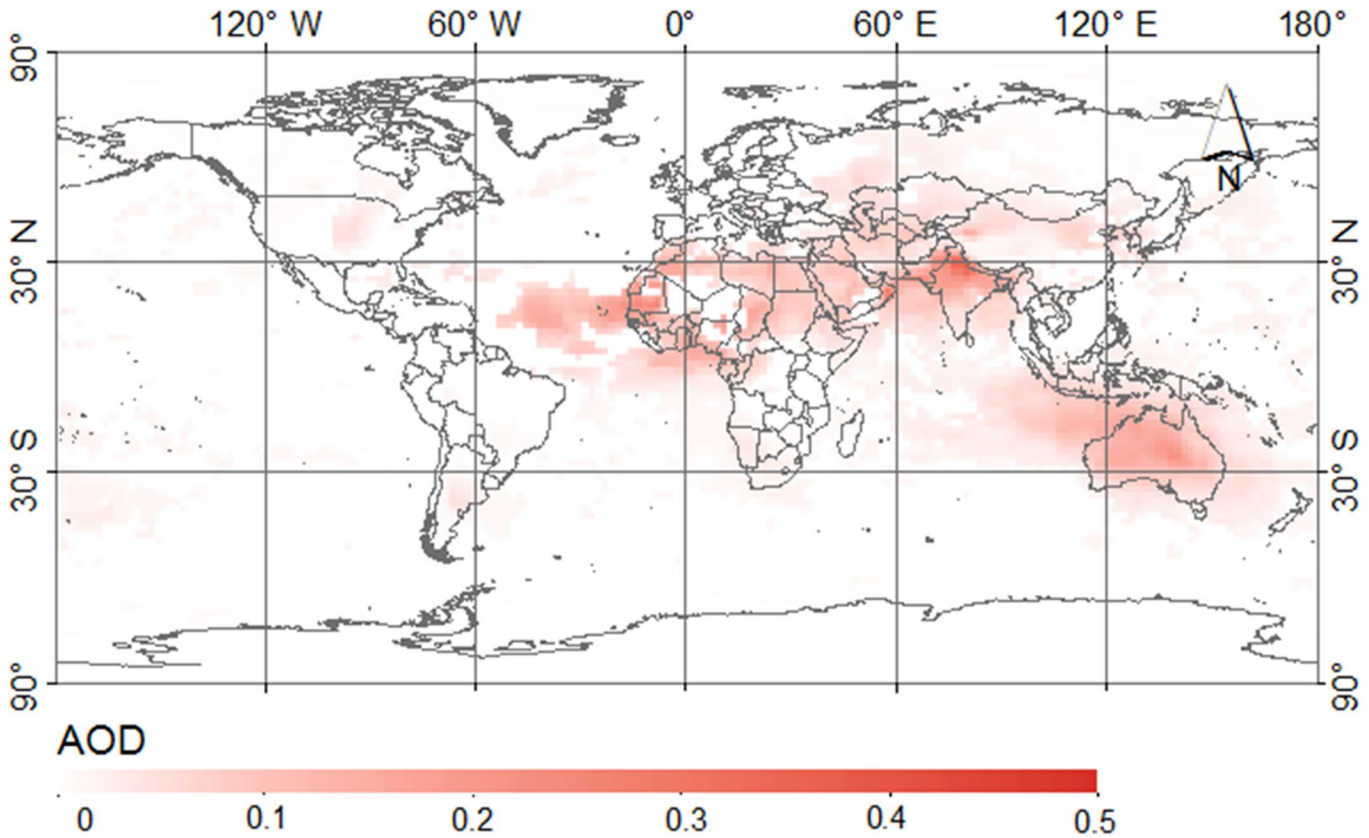

Extended Data Fig. 5 | Impact of biocrusts on dust aerosol optical depth (AOD). Relative hypothetical change of dust AOD upon complete removal of biocrusts obtained with the ECHAM6-HAM2-BIOCRUST model, accounting for a mean effect of biocrusts on TFV.

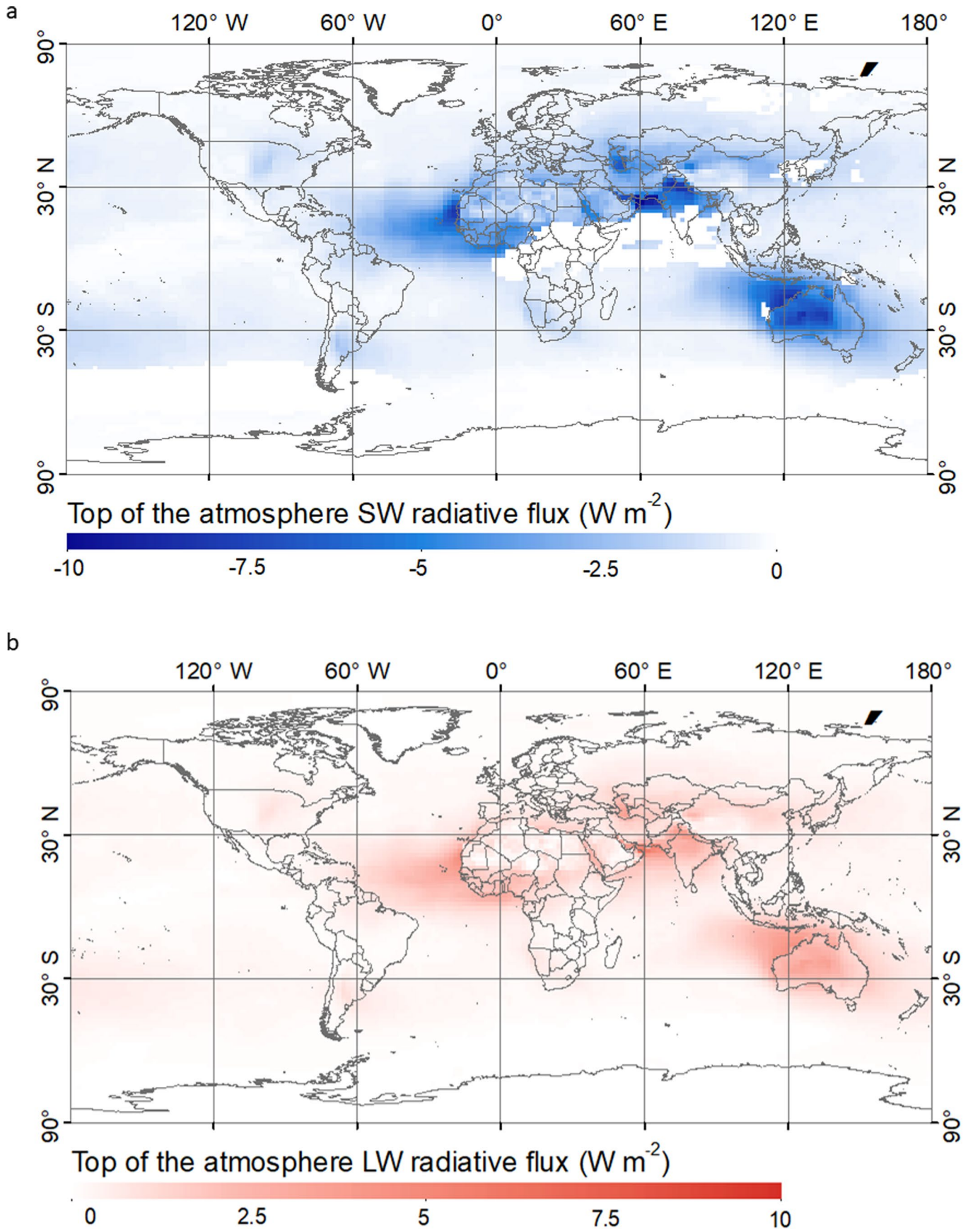

Extended Data Fig. 6 | Radiative effect of biocrusts at the top of the atmosphere. Hypothetical change of mean **(a)** short wave (SW), and **(b)** long wave (LW) aerosol radiative balance upon complete removal of biocrusts.

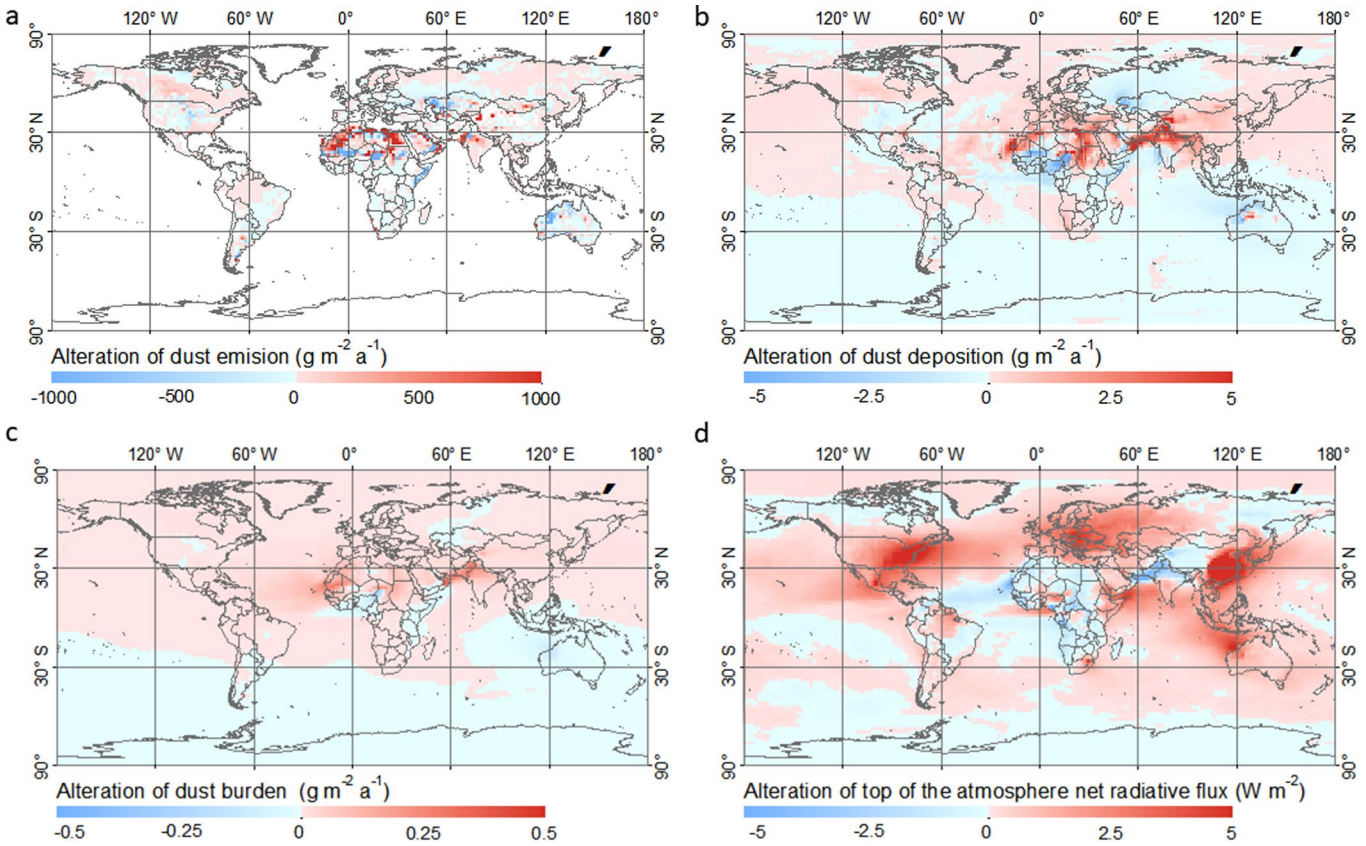

Extended Data Fig. 7 | Effect of global change and the induced biocrust cover loss estimated by 2070 on future dust cycling. Change of future **(a)** total annual dust emission, **(b)** total annual dust deposition, **(c)** mean annual atmospheric dust burden, and **(d)** mean annual aerosol net radiative effect at the top of the atmosphere. Data calculated according to the representative concentration pathway RCP4.5.

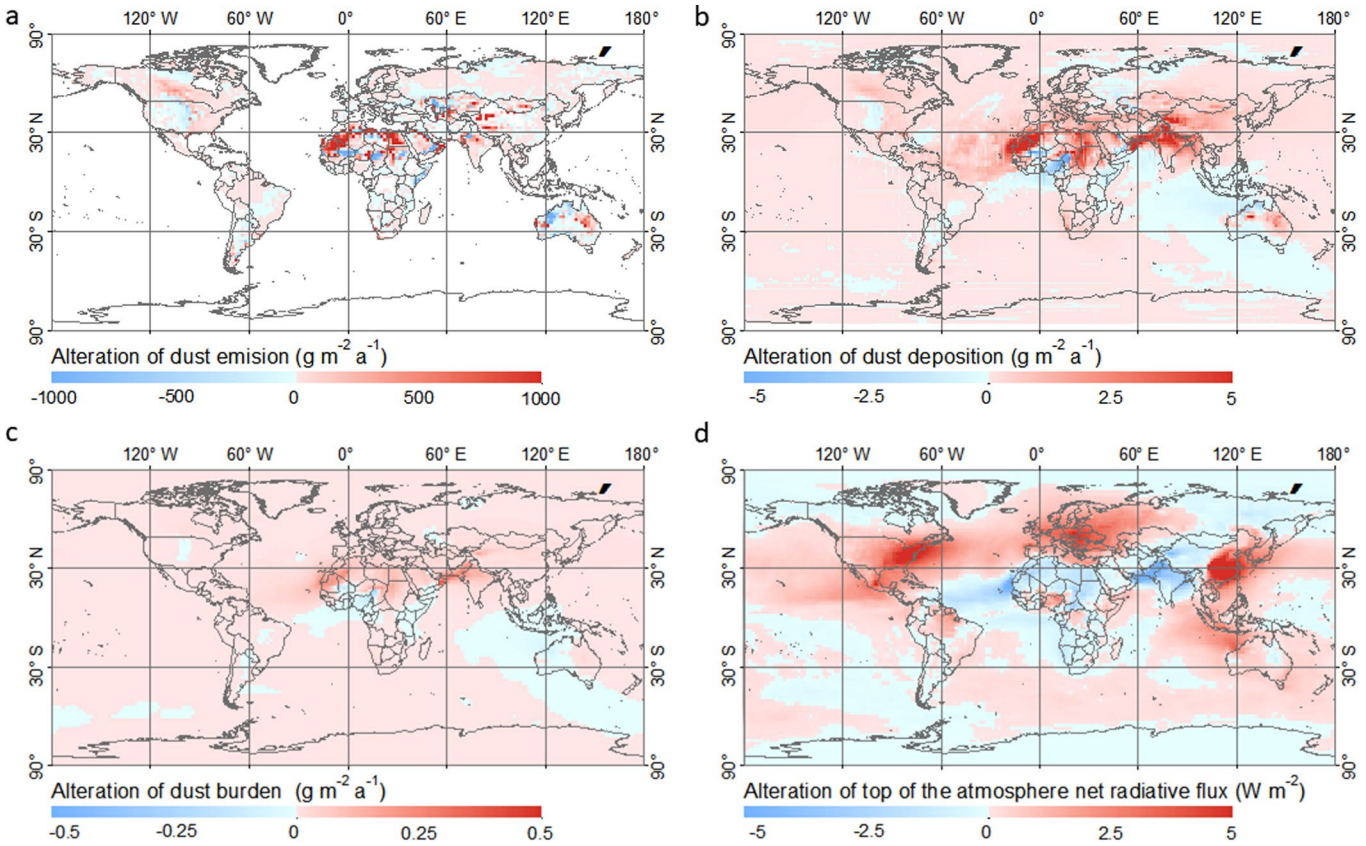

Extended Data Fig. 8 | Effect of global change and the induced biocrust cover loss estimated by 2070 on future dust cycling. Change of future **(a)** total annual dust emission, **(b)** total annual dust deposition, **(c)** mean annual atmospheric dust burden, and **(d)** mean annual aerosol net radiative effect at the top of the atmosphere. Data calculated according to the representative concentration pathway RCP8.5.

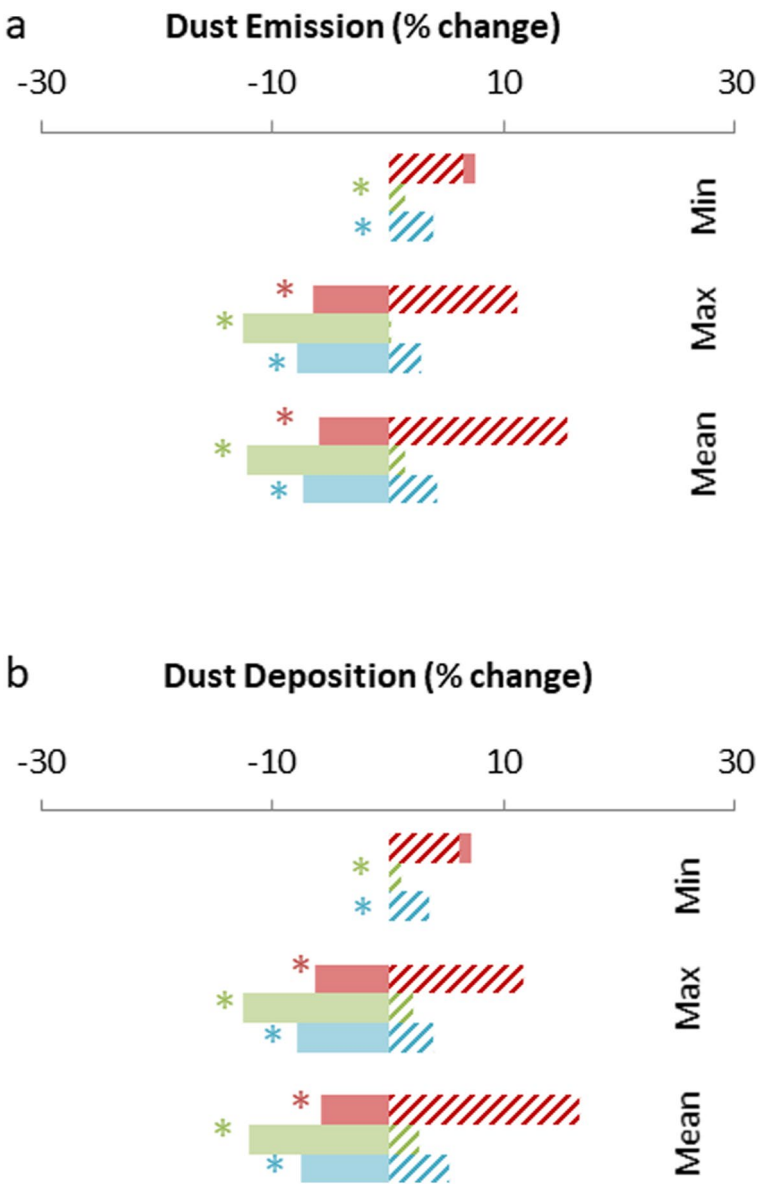

Extended Data Fig. 9 | Effect of future climate and anthropogenically induced biocrust cover loss estimated by 2070 on future dust cycling. Difference between current and future annual **(a)** dust emission, and **(b)** dust deposition, accounting for expected future changes in climate and biocrust cover (striped bars) compared to future simulations not including changes in biocrust cover (solid bars). Red, green and blue bars represent RCP2.6, RCP4.5 and RCP8.5, respectively. Statistically significant differences are indicated by an Asterisk (significance level: $p < 0.01$).